IJHSR
ijhighschoolresearch.org
RESEARCH ARTICLE

Constraint-Based Geospatial Analysis for Mars Landing Site Selection

Jia Shenai

Metea Valley High School, 1801 N Eola Rd, Aurora, IL 60502;

ABSTRACT: Often called the "seven minutes of terror," EDL (Entry, Descent, and Landing) is usually considered the riskiest phase of a Mars mission. Due to the limited time for corrective actions and the lack of margin for error in the descent sequence, it is imperative that surface conditions be carefully analyzed before site selection. This research uses environmental and topographical data from the MCD (Mars Climate Database) and MOLA (Mars Orbiter Laser Altimeter), respectively, to identify suitable regions on Mars for potential landings based primarily on engineering constraints. We evaluate elevation (to maximize atmospheric braking), slope (to ensure stable landings), and latitude (to support thermal stability and solar power usage). Our analysis identified several candidate landing zones that meet these criteria, including Amazonis Planitia, Chryse Planitia, Noctis Labyrinthus, and western Isidis Planitia. These results provide a preliminary, engineering-focused list that could guide early-stage mission planning, where the consequences of an unsuitable landing site could be catastrophic mission failure or loss of scientific return.

KEYWORDS: Engineering Mechanics, Aerospace and Aeronautical Engineering, Mars Landing Sites, Geospatial Analysis, Planetary Surface Conditions.

Introduction

As Mars exploration advances toward more complex scientific and crewed missions, selecting landing sites that are both scientifically valuable and operationally safe has become a central challenge. The success of any Mars surface mission relies upon the performance of the Entry, Descent, and Landing (EDL) system, which must function autonomously in real-time.[1] The EDL period is often called the "seven minutes of terror." During this short window, landing systems must manage atmospheric entry, deceleration, hazard detection, and touchdown, all while contending with uncertain, harsh environmental conditions.

Landing site selection is a constraint satisfaction problem, where criteria such as surface elevation, slope, and latitude impose limits on mission design. For instance, surface elevation affects atmospheric density, which influences drag forces during descent and the effectiveness of aerobraking mechanisms. Sites situated lower relative to the Mars areoid (Mars' equivalent to sea level) provide greater atmospheric depth, allowing for safer deceleration profiles. This constraint has been adopted in both recent NASA missions and current ESA planning models.[2,3] Slope is another critical factor, as high slopes increase the likelihood of post-landing instability or uneven load distribution, which may interfere with payload deployment or even tip the lander.[4] Latitude also plays a crucial role in mission planning. Sites closer to the equator benefit from more stable thermal conditions and greater solar energy availability, both factors that influence both thermal control systems and the viability of solar-powered payloads.[2,3]

Numerous past studies and missions, such as Mars Pathfinder, Spirit, Opportunity, Curiosity, and Perseverance, utilized planetary datasets such as the Mars Orbiter Laser Altimeter (MOLA) for topography and slope analysis and the Mars Climate Database (MCD) for environmental modeling.[5,6] MOLA data was collected by the Mars Orbiter Laser Altimeter aboard NASA's Mars Global Surveyor between 1997 and 2001, providing high-resolution topographic measurements.[5] MCD is a numerical model of Mars' climate, compiled from multiple spacecraft observations including Mars Global Surveyor, Mars Odyssey, and Mars Reconnaissance Orbiter, maintained by the Laboratoire de Météorologie Dynamique.[6]

In this study, using data from MOLA and MCD, we identify surface regions on Mars that meet key engineering constraints for safe landings. Any region exceeding defined thresholds for elevation, slope, or latitude is removed from consideration. The resulting maps highlight candidate zones that satisfy all considered EDL-related constraints simultaneously, providing a technically grounded starting point for future robotic or human mission planning. This study is intended as a first-pass, constraint-based geospatial screening tool using global datasets, rather than a final landing-site certification. In Section 2, we discuss the methods used to analyze the data and create the final map. In Section 3, we discuss the results and areas of scientific interest, which are then compared to historical successful and failed landings in Section 4.

Methods

2.1. Methodology:

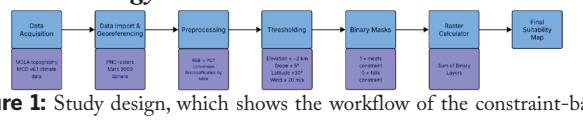

Figure 1: Study design, which shows the workflow of the constraint-based geospatial analysis used in this study, showing data sources, preprocessing steps, thresholding, raster overlay, and final landing-zone map. This workflow reduces the planet's surface to regions that are potentially safest for EDL.

DOI: 10.36838/IJHSR89.250

We use QGIS 3.42 for processing to identify regions of Mars that are suitable for landing (based on terrain slope, elevation, wind speed, and latitude),[7] as summarized in Figure 1. The analysis draws data from the Mars Climate Database (MCD) and Mars Orbiter Laser Altimeter (MOLA), processed into raster layers for geospatial filtering.

2.2. Data Acquisition:

Environmental and topographical data were obtained in PNG format from the Mars Climate Database (version 6.1) and NASA's MOLA dataset.[5,6,14] The data sources, resolutions, coordinate systems, and units used in this analysis are summarized in Table 1. Each PNG was uploaded to QGIS as a raster layer. We georeferenced each layer to the Mars 2000 Sphere coordinate system using known latitude and longitude points. A raster represents data as a grid of pixels, where each pixel stores a value for a surface property. The RGB rasters were then converted to pseudocolor (PCT) format using the "RGB to PCT" tool. Pseudocolor maps colors to numeric ranges to enable interpretation and analysis. Converting RGB to pseudocolor standardizes the color-mapping. Each color corresponds to a single numeric value, which enables consistent reclassification. These integer values do not correspond to the dataset's physical units, so we reclassified the values using the "Reclassify by Table" tool to map each color value to its actual data value based on the dataset's key, following the MCD v6.1 documentation.[14]

Table 1: Summarizes the data sources, coordinate system, spatial resolution, and units for each raster layer used in this analysis. These datasets provide global coverage suitable for regional-scale landing-site screening.

Constraint	Dataset and Source	Coordinate System	Resolution	Ranges	Units
Elevation	Global Topography (MOLA)	Mars 2000 Sphere	128 pixels/degree (~463 m at equator)	-8 to >+12 km	km (relative to Martian areoid)
Slope	Surface Slope (MCD v6.1)	Mars 2000 Sphere	32 pixels/degree (~1.85 km at equator)	0° to 22°	Degrees
Latitude	Latitude	Mars 2000 Sphere	Global	-90 to +90	Degrees
Wind Speed	Near-surface mean wind speed (MCD v6.1)	Mars 2000 Sphere	32 pixels/degree (~1.85 km at equator)	0.1 to 89.9 m/s	m/s

2.3. Thresholds:

Elevation: ≤ -2 km (mars areoid)

To increase atmospheric column density during EDL, we restrict candidate terrain to low elevations. Past missions set mission-specific limits in this direction: the Mars Exploration Rovers (MER) required elevation < –1.3 km (MOLA areoid)[4]; InSight's engineering guidance targeted even lower terrain (< –2.5 km) for additional deceleration margin[8], and in fact InSight touched down at ~–2.61 km[9]. EDL reviews also note that higher landing altitudes push system performance, especially as landed mass grows.[1] In this study, we therefore adopt a baseline threshold of ≤ –2.0 km, which sits within the envelope used by recent missions and provides a conservative margin without excluding too much scientifically interesting terrain.

Slope: ≤ 5°

Engineering slope thresholds are scale-dependent, with different limits commonly applied at kilometer, hectometer, and meter scales. For instance, small-scale slopes can provide information about smaller obstacles like boulders and steep crater walls, while at the kilometer scale, large regional slopes can create issues with stability and traversability. Given the kilometer-scale resolution of the dataset used here (~1.85 km/pixel), the ≤5° threshold is applied as a conservative regional screening criterion rather than as a measure of local landing hazards.

Latitude: –30° to +30°

Latitude controls thermal environment and solar power. MER targeted low latitudes for energy (about 10°N to 15°S)[10], ExoMars set 5°S–25°N for power/thermal reasons, and the Mars 2020 mission material shows access and planning commonly within ±30°, even though the EDL system could reach farther.[11] Following these missions, we use -30° to +30° to support thermal stability and year-round solar energy.

Wind Speed: ≤ 20 m/s (near-surface mean)

Winds add cross-range under the parachute and can complicate terminal descent. Engineering guides usually set caps rather than averages: MSL planned for steady surface winds up to ~15 m/s with gusts to ~30 m/s, and ExoMars used ≤25 m/s near the ground during descent and operations.[3,10] Actual measurements at Phoenix and at Jezero crater show typical mean winds of only a few to ~10 m/s, with stronger gusts during dust activity.[12,13] Since our MCD layer is a mean rather than a maximum, we keep regions with ≤20 m/s to stay below those caps while not over-screening.

2.4. Data Analysis:

Next, we applied the thresholds to each criterion explained in Section 2.3. Each reclassified raster layer became a binary mask: 1 indicating the threshold was met, and 0 indicating it was not met. To identify areas meeting multiple constraints, we used the Raster Calculator tool. We summed the four binary masks in Raster Calculator, producing a raster where each pixel value (0-4) equals the number of constraints satisfied using the following equation: ("BinaryElevation@1") + ("BinarySlope@1") + ("BinaryWindSpeed@1") + ("BinaryLatitude@1"). This analysis applies thresholding and raster overlay; no statistical hypothesis tests or predictive statistical models were performed.

■ Results

3.1. Final Global Landing-Site Suitability Map:

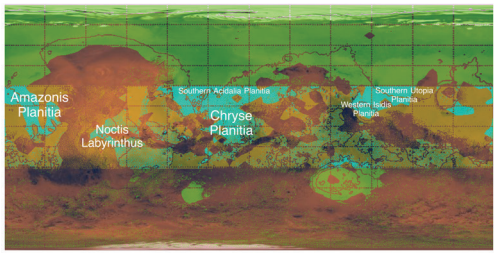

Figure 2: The final landing-zone suitability map, derived from four constraints: elevation ≤ -2 km (relative to the Martian areoid), slope ≤ 5° (degrees), latitude within ±30° (degrees), and mean near-surface wind speed ≤ 20 m/s, based on MOLA topography and MCD v6.1 climate data. Cyan indicates pixels meeting all four constraints; green indicates pixels meeting all of the constraints except latitude; yellow indicates pixels within ±30° latitude that fail at least one of the other constraints. The map shows that the most suitable landing regions (cyan) occur primarily in large low-elevation basins such as Amazonis Planitia, Chryse Planitia, and western Isidis Planitia.

The areas in cyan in Figure 2 stand out because they have low elevations, which enables thicker atmospheres for EDL, are relatively flat over large scales, have low wind speed, and are low latitude.[1-4, 8, 10] Other parts of Mars are excluded either by slope, elevation, wind speed, or latitude. Among regions meeting all four constraints (cyan), Amazonis Planitia contains the largest and most continuous suitable area, followed by Chryse Planitia and western Isidis Planitia. Noctis Labyrinthus and parts of southern Acidalia and Utopia Planitia retain smaller, more fragmented cyan regions.

Table 2: Details the surface area of Mars retained after applying each constraint and its combined intersection. Applying all four constraints simultaneously reduces the viable landing area to approximately 1.3×10^7 km^2.

Constraint	Retained area (km²)	% of Mars surface
Elevation ≤ −2 km	74,000,000	51.1
Latitude (±30°)	72,200,000	50.0
Slope ≤ 5°	123,000,000	85.0
Wind speed ≤ 20 m/s	83,300,000	57.5
All four constraints (cyan region)	13,000,000	9.0

Table 2 displays the actual impact of each constraint and the combined area of the regions retained as most promising. Individually, slope is the least restrictive criterion, as it retains approximately 85% of the Martian surface, while elevation and near-surface wind speed each retain roughly half of the planet. The latitude band (±30°) encompasses exactly 50% of Mars' surface area. When all four constraints are applied simultaneously, the retained surface area is reduced to approximately 1.30×10^7 km^2, corresponding to about 9% of the total Martian surface and 18% of the ±30° latitude band.

3.2. Explanation of Areas Retained:

The regions highlighted in cyan on the final suitability map emerge because they simultaneously satisfy all four engineering constraints, each of which removes a different type of EDL risk. Aside from latitude, low elevation is the most restrictive constraint globally and plays a primary role in shaping the spatial pattern of suitable terrain. As such, large basins such as Amazonis Planitia, Chryse Planitia, and western Isidis Planitia, which lie several kilometers below the Martian areoid (providing a thicker atmospheric column during entry), constitute the majority of areas retained. Slope further refines the candidate regions by excluding areas with significant regional tilts, particularly around crater rims, volcanic constructs, and heavily fractured terrains. Regions that pass the slope constraint tend to be smooth volcanic plains (like Amazonis Planitia) or sediment-filled basins (like Chryse Planitia), since those areas have undergone extensive resurfacing.

To reiterate, latitude primarily acts as a secondary planning constraint rather than a strict EDL one. Regions within ±30° latitude are favored because they experience more stable temperatures and have higher average solar energy availability. Several candidate regions extend beyond this latitude band, but are excluded from the cyan mask due to thermal and operational considerations rather than landing safety alone. This distinction is reflected in the green regions of the map, which satisfy all engineering constraints except latitude.

Wind speed provides an additional screening effect that excludes regions influenced by stronger near-surface atmospheric circulation. While much of Mars experiences relatively low mean surface winds, elevated terrain and topographic boundaries can enhance wind speeds.

3.3. Areas of Scientific Interest:

Within these safe zones, there are many areas of scientific interest. While these sites were not selected based on science criteria, these areas have a lot of potential for missions with great scientific return.

Some examples include Isidis Planitia, Noctis Labyrinthus, and Chryse Planitia. The western margin of Isidis Planitia, especially the Nili Fossae region and Jezero crater, exposes rock units that contain olivine together with carbonates, and a well-preserved river delta that entered a crater lake. These features indicate that water likely interacted with the rocks under neutral to alkaline conditions (as opposed to strongly acidic water) and that rivers delivered sediment to the lake over an extended period, building the delta through sustained deposition.[15-17] In Noctis Labyrinthus, orbital data detect phyllosilicates (clays), sulfates (salts that often form as water evaporates), and hydrated silica (silica containing water) on trough floors and walls. Finding these minerals together indicates water–rock environments.[18,19] Chryse Planitia sits at the ends of the circum-Chryse outflow channels and preserves deposits from very large floods. Recent studies also suggest that a pre-existing topographic low helped guide channel formation and later resurfacing of the basin, with possible marine or glacial influences on that evolution.[20-22]

■ Discussion

4.1. Validation:

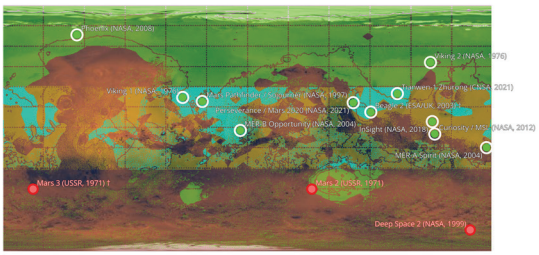

Figure 3: Landing-zone suitability map (elevation ≤ −2 km; slope ≤ 5°; latitude within ±30°; mean near-surface wind ≤ 20 m/s) with historical landing locations overlaid. Green points represent missions that achieved a successful landing; red points represent missions that had a hard/failed landing.[21-23] Most successful landings fall within the cyan or green regions, which supports the validity of the suitability mask as an early-stage engineering screen for Mars landing site selection.

To validate the candidate regions identified in Section 3 in context, we compare them with the locations of historical Mars landings. Historical landings validate our results. Of the eleven successful landings on Mars, seven fall within the cyan regions (meeting all four constraints). These include Viking 1 Mars Pathfinder, Spirit and Opportunity, Perseverance, and China's Zhurong rover.[4, 10, 16, 23-25] Two successful missions (Phoenix and Viking 2) fall within the green regions, which indicates that they meet the elevation, slope, and wind constraints but lie outside the ±30° latitude band.[26, 27] This is expected because the latitude criterion is not strictly an EDL limit but was con-

DOI: 10.36838/IJHSR89.250

sidered due to the mission-planning preferences of a thermal environment and solar-energy availability. Phoenix was designed specifically for a high-latitude science target, and the effects of landing at a high latitude were lessened because it operated during polar summer. Two other successful missions (InSight and Curiosity) fall within the yellow regions, indicating that at least three of the four constraints were met.[28,29] Overall, 64% of successful landings fell within the cyan regions, and 82% fell within the cyan and green regions. The fact that most successful landings occur within cyan regions supports the suitability mask as an early-stage screen, while the exceptions highlight the importance of mission-specific design and higher-resolution follow-on analysis.

Red points denote missions that had a hard landing or mission failure, including Deep Space 2, which failed largely due to communication issues, and Mars 2 and Mars 3.[30,31] Mars 3 successfully made a soft landing, but lost communications soon after, highlighting that landing outcomes are influenced by multiple variables beyond the coarse environmental constraints modeled here. Overall, all of the failed landings occurred outside the cyan, green, or yellow regions.

Future work can extend this analysis by incorporating higher-resolution hazard datasets, such as HiRISE and CTX stereo-derived digital elevation models, to capture boulder distributions, small craters, and surface roughness at lander scales.

4.2. Limitations and Scope of the Analysis:

This analysis is not intended to be a final landing-site certification. It is an early-stage engineering screen. The main limitations present in this analysis are the resolution of the datasets and the usage of the mean near-surface wind without any other wind-related constraints. The datasets used (MOLA topography and MCD v6.1) are global, and also somewhat coarse in spatial resolution, which means that the resulting masks capture regional-scale conditions rather than local hazards. Critical EDL risks, such as meter-scale slopes, boulder distributions, small craters, and surface roughness, occur at smaller scales (~1–10 m), which are not resolved by the datasets used here. As such, regions this analysis identifies as suitable will still later require further assessment, such as high-resolution hazard mapping. Additionally, the usage of mean near-surface wind speed as the only wind-related constraint does not take into account transient gusts or dust-storm-driven extremes, which are also crucial to landing site selection, further underscoring that this approach is designed to narrow candidate regions rather than certify landing safety.

■ Conclusion

This study demonstrates that a constraint-driven approach using MOLA topography and MCD environmental data can effectively identify Mars surface regions meeting critical EDL safety requirements. By applying conservative thresholds for elevation, slope, latitude, and surface wind speed, we created a set of candidate landing zones with favorable engineering characteristics. These areas align with parameters used in past successful missions and also encompass terrains of high potential scientific value.

The results provide a methodology that can inform early mission planning, narrowing the options of possible sites before using finer-resolution hazard mapping, considering scientific objectives, and resources. In practice, mission planning could involve using the cyan mask (Figure 2) as a first-pass filter to narrow a large set of candidate landing ellipses: ellipses falling largely outside the cyan regions would be deprioritized early, while ellipses overlapping cyan regions would advance to more detailed hazard assessment. Selecting a landing site would also entail further assessment of regions using high-resolution data (e.g., HiRISE/CTX stereo DEM acquisition and boulder/roughness mapping) within the most promising identified regions. This same process can also be rerun with mission-specific adjustments to the constraints (e.g., a narrower latitude band for a solar-powered mission or a different wind criterion) to rapidly generate an updated candidate set before detailed landing-site certification. Using geospatial analysis with EDL engineering constraints offers a structured pathway to reduce mission risk. By prioritizing sites that meet safety thresholds at the earliest stages of planning, future Mars missions can increase their margin for success.

Some next steps include substituting PNGs with native numeric MOLA and MCD gridded data to improve the precision of reclassification, extending the wind screening beyond a single mean near-surface layer by testing seasonality and stronger-wind scenarios (e.g., different seasons/local times in MCD) to better reflect extremes, and doing further analysis using higher-resolution terrain and hazard datasets (e.g., CTX/HiRISE stereo DEMs) to assess meter-scale slopes, roughness, and boulder fields within the candidate cyan regions identified here.

■ Acknowledgments

I would like to thank Dr. Chima McGruder and Catherine Petretti for their invaluable guidance, feedback, and expertise throughout the course of my research. I am also incredibly grateful to my parents for their constant support and encouragement.

■ References

1. Braun, R. D.; Manning, R. M. Mars Exploration Entry, Descent, and Landing Challenges. J. Spacecr. Rockets 2007, 44, 310–323. https://doi.org/10.2514/1.25116
2. Golombek, M. P.; Grant, J. A.; Kipp, D. M.; Vasavada, A. R.; Kirk, R. L.; Fergason, R. L.; *et al.* Selection of the Mars Science Laboratory Landing Site. Space Sci. Rev. 2012, 170, 641–737. https://doi.org/10.1007/s11214-012-9916-y
3. European Space Agency. ExoMars 2018 Landing Site Selection: User's Manual; Ref. EXM-SCI-LSS-ESA/IKI-003, Version 1.0; European Space Agency, 2013.https://sci.esa.int/documents/33431/35950/1567258130694-ExoMars_LSS_User_Manual_V1_17Dec13.pdf
4. Golombek, M. P.; Grant, J. A.; Parker, T. J.; Kass, D. M.; Crisp, J. A.; Squyres, S. W.; *et al.* Selection of the Mars Exploration Rover Landing Sites. J. Geophys. Res. Planets 2003, 108 (E12), 8072. https://doi.org/10.1029/2003JE002074
5. Smith, D. E.; Zuber, M. T.; Frey, H. V.; Garvin, J. B.; Head, J. W.; Muhleman, D. O.; *et al.* Mars Orbiter Laser Altimeter (MOLA): Experiment Summary after the First Year of Global Mapping of

Mars. J. Geophys. Res. Planets 2001, 106 (E10), 23689–23722. https://doi.org/10.1029/2000JE001364
6. Forget, F.; Hourdin, F.; Fournier, R.; Hourdin, C.; Talagrand, O.; Collins, M.; *et al.* Improved General Circulation Models of the Martian Atmosphere from the Surface to Above 80 km. J. Geophys. Res. Planets 1999, 104 (E10), 24155–24175. https://doi.org/10.1029/1999JE001025
7. QGIS Development Team. QGIS Geographic Information System (Version 3.42) [Computer software]; QGIS Association, 2025. https://www.qgis.org
8. Golombek, M. P.; Kipp, D.; Warner, N.; Daubar, I. J.; Fergason, R.; Kirk, R. L.; *et al.* Selection of the InSight Landing Site. Space Sci. Rev. 2017, 211, 5–95. https://doi.org/10.1007/s11214-016-0321-9
9. Golombek, M. P.; Warner, N. H.; Grant, J. A.; Hauber, E.; Ansan, V.; Weitz, C. M.; *et al.* Geology of the InSight Landing Site on Mars. Nat. Commun. 2020, 11, 1014. https://doi.org/10.1038/s41467-020-14679-1
10. Crisp, J. A.; Adler, M.; Matijevic, J.; Squyres, S. W.; Arvidson, R. E.; Kass, D. M.; *et al.* Mars Exploration Rover Mission. J. Geophys. Res. Planets 2003, 108 (E12), 8061. https://doi.org/10.1029/2002JE002038
11. Jet Propulsion Laboratory. MSL Landing Site Selection: User's Guide to Engineering Constraints, Version 4.5.1; Jet Propulsion Laboratory, California Institute of Technology: Pasadena, CA, 2007. https://marsoweb.nas.nasa.gov/landingsites/msl/memoranda/MSL_Eng_User_Guide_v4.5.1.pdf
12. Holstein-Rathlou, C.; Gunnlaugsson, H. P.; Merrison, J. P.; Bean, K. M.; Cantor, B. A.; Davis, J. A.; *et al.* Winds at the Phoenix Landing Site. J. Geophys. Res. Planets 2010, 115, E00E18. https://doi.org/10.1029/2009JE003411
13. Viúdez-Moreiras, D.; Lemmon, M.; Newman, C. E.; Guzewich, S.; Mischna, M.; Gómez-Elvira, J.; *et al.* Winds at the Mars 2020 Landing Site. 1. Near-Surface Wind Patterns at Jezero Crater. J. Geophys. Res. Planets 2022, 127, e2022JE007522. https://doi.org/10.1029/2022JE007522
14. Millour, E.; Forget, F.; Pierron, T.; Lewis, S. R.; *et al.* Mars Climate Database v6.1: User Manual; October 2022. https://www-mars.lmd.jussieu.fr/mars/info_web/user_manual_6.1.pdf
15. Ehlmann, B. L.; Mustard, J. F.; Swayze, G. A.; Clark, R. N.; Bishop, J. L.; Poulet, F.; *et al.* Orbital Identification of Carbonate-Bearing Rocks on Mars. Science 2008, 322, 1828–1832. https://doi.org/10.1126/science.1164759
16. Mangold, N.; Stack, K. M.; Le Deit, L.; Grotzinger, J. P.; Horgan, B.; Williams, R. M. E.; *et al.* Perseverance Rover Reveals an Ancient Delta–Lake System at Jezero. Science 2021, 374, 711–717. https://doi.org/10.1126/science.abg9067
17. Caravaca, G.; Mangold, N.; Stack, K. M.; Grotzinger, J. P.; Rivera-Hernández, F.; Bennett, K.; *et al.* Architecture of Fluvial and Deltaic Deposits Exposed along the Eastern Edge of the Western Fan of Jezero Crater. J. Geophys. Res. Planets 2024, 129, e2023JE008204. https://doi.org/10.1029/2023JE008204
18. Thollot, P.; Mangold, N.; Ansan, V.; Le Mouélic, S.; Bishop, J. L.; Weitz, C. M.; *et al.* Most Mars Minerals in a Nutshell: Various Alteration Phases Formed in a Single Environment in Noctis Labyrinthus. J. Geophys. Res. Planets 2012, 117, E00J06. https://doi.org/10.1029/2011JE004028
19. Weitz, C. M.; Bishop, J. L.; Noe Dobrea, E. Z.; Thomson, B. J.; Perry, K. A.; Seelos, K. D.; *et al.* Diverse Mineralogies in Noctis Labyrinthus, Mars: Evidence for Aqueous Processes. Planet. Space Sci. 2013, 87, 130–145. https://doi.org/10.1016/j.pss.2013.09.002
20. Coleman, N. M. Aqueous Flows Carved the Outflow Channels on Mars. J. Geophys. Res. Planets 2003, 108 (E5), 5039. https://doi.org/10.1029/2002JE001940
21. Pan, L.; Ehlmann, B. L.; Carter, J.; Allen, C.; Horgan, B.; Bishop, J. L.; Brown, A. J.; *et al.* Impact Origin and Evolution of Chryse Planitia Revealed by Buried Craters. Nat. Commun. 2019, 10, 4050. https://doi.org/10.1038/s41467-019-12162-0
22. Rodríguez, J. A. P.; Fairén, A. G.; Tanaka, K. L.; Zarroca, M.; Linares, R.; Platz, T.; Miyamoto, H.; Koster van Groos, A.; *et al.* Marine/Glacial Influences in Circum-Chryse: Implications for Basin Resurfacing. Sci. Rep. 2015, 5, 13404. https://doi.org/10.1038/srep13404
23. Binder, A. B.; Jones, K. L.; Boyce, J. M.; Davis, P. A.; Duxbury, T. C.; Hartmann, W. K.; *et al.* The Geology of the Viking Lander 1 Site. J. Geophys. Res. 1977, 82 (28), 4439–4451. https://doi.org/10.1029/JS082i028p04439
24. Golombek, M. P.; Anderson, R. C.; Barnes, J. R.; Bell, J. F.; Bridges, N. T.; Britt, D. T.; *et al.* Overview of the Mars Pathfinder Mission: Launch through Landing, Surface Operations, Data Sets, and Science Results. J. Geophys. Res. Planets 1999, 104, 8523–8553. https://doi.org/10.1029/98JE02554
25. Wu, B.; Di, K.; Wang, J.; Hu, W.; Liu, Z.; Gou, S.; Yue, Z.; He, Z.; Wan, W.; *et al.* Landing Site Selection and Characterization of Tianwen-1 Zhurong Rover on Mars. J. Geophys. Res. Planets 2022, 127, e2021JE007137. https://doi.org/10.1029/2021JE007137
26. Smith, P. H.; Tamppari, L. K.; Arvidson, R. E.; Bass, D.; Blaney, D.; Boynton, W. V.; *et al.* Introduction to Special Section: Phoenix Mission. J. Geophys. Res. Planets 2008, 113, E00A18. https://doi.org/10.1029/2008JE003083
27. Mutch, T. A.; Arvidson, R. E.; Binder, A. B.; Guinness, E. A.; Morris, E. C. The Geology of the Viking Lander 2 Site. J. Geophys. Res. 1977, 82 (28), 4452–4467. https://doi.org/10.1029/JS082i028p04452
28. Karlgaard, C. D.; Kutty, P.; Schoenenberger, M.; Shidner, J.; Little, A.; *et al.* Mars InSight Entry, Descent, and Landing Trajectory and Atmosphere Reconstruction. In AIAA Scitech 2020 Forum; American Institute of Aeronautics and Astronautics: Reston, VA, 2020; Paper 2020-1271. https://doi.org/10.2514/6.2020-1271
29. Vasavada, A. R.; Stack, K. M.; Grotzinger, J. P.; Gupta, S.; Grant, J. A.; Calef, F.; Farley, K. A.; *et al.* Mission Overview and Scientific Contributions from the Mars Science Laboratory Curiosity Rover after Eight Years of Surface Operations. Space Sci. Rev. 2022, 218, 14. https://doi.org/10.1007/s11214-022-00882-7
30. Smrekar, S. E.; Catling, D. C.; Lorenz, R. D.; Magalhães, J.; Moersch, J.; Morgan, P.; Murray, B.; Presley, M.; Yen, A.; Zent, A.; Blaney, D. Deep Space 2: The Mars Microprobe Mission. J. Geophys. Res. Planets 1999, 104 (E11), 27013–27030. https://doi.org/10.1029/1999JE001073
31. JPL Special Review Board. Report on the Loss of the Mars Polar Lander and Deep Space 2 Missions; JPL D-18709; Jet Propulsion Laboratory, California Institute of Technology: Pasadena, CA, 2000. https://ntrs.nasa.gov/api/citations/20000061966/downloads/20000061966.pdf

Authors

Jia Shenai is a junior at Metea Valley High School in Aurora, Illinois, with a strong passion for engineering and design. She hopes to pursue astronautical engineering, and she envisions contributing to space exploration and advancing innovative technologies that shape humanity's future beyond Earth

DOI: 10.36838/IJHSR89.250